SPiraL Aggregation Map (SPLAM): A new descriptor for robust template matching with fast algorithm ☆

Huang-Chia Shih [a,b,*], Kuan-Chun Yu [a,b]

[a] Human–Computer Interaction Multimedia Laboratory, Department of Electrical Engineering, Yuan Ze University, Taoyuan, Taiwan, ROC
[b] Innovation Center for Big Data and Digital Convergence, Yuan Ze University, Taoyuan, Taiwan, ROC

ABSTRACT

This paper describes a robust template matching algorithm undergoing rotation–scaling–translation (RST) variations via our proposed SPiraL Aggregation Map (SPLAM), which is a novel image warping scheme. It not only provides an efficient method for generating the desired projection profiles for matching, it also enables us to determine the rotation angle, and is invariant to scale changes. Compared to other model-based methods, the proposed spiral projection model (SPM) provides the structural and statistical information about the template in a more general and easier to comprehend format. The SPM is a model-based texture-description scheme that enables the simultaneous representation for each value of projection profile. The profile, a set of parametric projection values functions by angular indexing, is the aggregate from a group of spiral sampling pixels. The experimental evaluation shows that the properties of the algorithm achieved very attractive results.

© 2014 Elsevier Ltd. All rights reserved.

1. Introduction

Advanced research and development in template matching has found numerous applications in areas such as image retrieval, near-duplicate detection, object detection and recognition with impressive performances. Template matching is a critical technique in many visual-based pattern recognition applications. Normally, the template matching procedure consists of two phases. In the first phase, the representative feature vectors of the template and the given test sub-image positions are extracted. In the second phase, the matching score is acquired using the similarity measure such as the sum of the absolute differences, the n-norm distance, and cross-correlation. However, the first phase usually dominates the robustness of the system performance. To cope with the template undergoing unpredictable geometric transformations, it is not surprising that the use of the invariant local descriptor is indispensable.

In practice, template matching usually suffers from problems of rotation, scaling, translation, and brightness/contrast changes. Conventional approaches are seldom able to handle these problems simultaneously, depending on the model. One of the most capable schemes for dealing with both rotation and scale invariant

properties is based on the cascade model. Kim and Araujo [1] showed a cascade framework in which ring projection method was used to deal with the rotation variation and the radial projection method was applied to estimate the local rotation angle.

1.1. Related work

Traditionally, template matching is divided into model-based and transformation-based methods. The model-based method focuses on extracting the intrinsic characteristics from a particular sampling model or projection path. The local structural information of the template can be preserved and enhanced using an appropriate descriptor that is insensitive to geometric transformations. For instance, the ring projection [2–6] is a simple algorithm that enables transforming 2-D patterns into 1-D profiles by circularly aggregating pixels on the same radius from the center point, in order to achieve rotation invariant features. Radial projection [7] is a sampling method from 2-D image pixels under radial lines into a 1-D profile as a function of the radial line angle. The 1-D profile obtained from the radial projection is normally invariant to scale changes. The orientation code (OC) [8] can be obtained by grouping the quantized values of the gradient angle around each pixel on the image. The OC is a type of rotation-discriminating feature; however it is not scale invariant for all situations. The shape context was proposed by Belongie et al. [9]. It encodes the edge points of the template based on a reference point under the log-polar coordinate. It is intrinsic invariant to translation and scaling, but is not efficient for rotation invariant

matching without some ad-hoc treatment of the template. Ojala et al. [10] used local binary patterns (LBP) in rotation-invariant texture classification. LBP can be treated as a general approach to the conventionally divergent structural and statistical models for texture analysis. Notable illumination-invariant LBP features for face recognition system were proposed by Li et al. [11].

On the other hand, the transformation-based method transforms the spatial image plane to the parameter plane using transformation methods with RST-invariant abilities such as the *Fourier transform* (FT) [12–14], *Wavelet transform* (WT) [15-16], *Radon transform* (RT) [17–19], *Mellin transform* (MT) [20] and others. The FT is one of the most popular techniques for dealing with the RST-invariance problem because it efficiently employs a fast algorithm. In Ref. [15], the authors illustrated an extension of the phase correlation technique in the Fourier-domain for achieving RST invariance, and applied for image registration. A frequency domain method to handle scale-invariant template matching in a single pass can be achieved using the MT [21]. To accommodate the limitations that the MT only provides scale-invariant matching, the *Fourier–Mellin transform* [22–24] extends phase correlation to handle images transformed by both translation and rotation. As a result, numerous research has combined the different transformations when handling many of the invariance situations. For instance, Hoang and Tabbone [25] used the RT, FT, and MT in pattern recognition. In Ref. [26], the RT and WT methods are combined to deal with texture analysis. The RT, dual-tree complex WT and FT are adopted in pattern recognition [27]. However, in the case of larger scale changes, it induces many noises in the Fourier coefficients when recovering the rotation, scale, and translation parameters. In Ref. [28], the authors show that the approach applies the frequency domain only when used in double-sized scaling.

Recently, combining the model-based and transformation-based scheme has been considered, such as in Refs. [29–31]. Amiri and Rabiee [29] extracted a set of coefficients as object features in the WT-domain, and applied the log-polar mapping model in the parametric template space to attain rotation/scale invariance. Apparently, the fusion framework significantly increased the complexity of the system, but was still unable to deal with the serious geometric changes. Thus, we focused on modeling the image directly in the spatial domain and recovered the best RST by performing a correlation on tiles that were projected into feature coordination called SPiraL Aggregation Map (SPLAM). We concentrated on solving the geometric variability due to the change in pose and the different angles of the viewpoint by using a single projective model called spiral projection model (SPM).

1.2. Motivations

This study focused on the model-based gray-scale template matching in order to understand more structural information from the template and to remove the computational burden from the transformation cost. As mentioned earlier, although the model-based approach such as the ring and radial projection methods show promising results in experiments, they have some unsolvable drawbacks. Although profiles of the ring projection method for object search has been used numerously for rotation-invariant template matching [4,32,33] they are not applicable in some situations, such as when the template has a circular symmetrical pattern with a radial appearance in a particular orientation, such as a clock, compass, color wheel and so on. In addition, each value of the projection profile is collected from a different number of sampling pixels which is a function of the radius. In other words, the spatial resolution sampling from the inner circle must be less than that of the outer circle. Each value of the projection profile is acquired from a different number of sampling pixels. However, it is very difficult to provide an equivalent sampling resolution for each of the values, making it impossible to accurately handle the overall error model.

1.2.1. Circular symmetry problem

Fig. 1(a) and (b) shows the original image and rotated 90° counterclockwise, respectively. Another case is where the changes of the hands are only shown in Fig. 1(c). If the ring projection applies for describing these three images, they will obtain the same projection profiles. It is not our intention to deny that the ring projection scheme is not good at attacking the rotation-invariance. Nevertheless, according to this example, it is unable to distinguish the rotation cases between the inside pattern and the entire image. A radial projection is required to solve this ambiguous situation.

1.2.2. Texture characteristics

In the scaling problem, the ring projection cannot obtain a stable result unless the direction-based interpolation or shrinking methods are adopted. Based on the definition of ring projection, each value of the profile is an aggregation from a different number of pixels of the template. If uniform sampling is applied to describe the image pattern, it will introduce unpredictable noise and will be unable to make a perfect match. The radial projection is a useful representation for solving scale variations. In general, a cross-correlation algorithm is followed by computing the projection profile to determine the orientation of the template. Compared to the ring projection, the radial projection has better properties because each value of the projection profile comes from the same number of pixels. However, it still has some shortcomings. The regular sampling in the radial direction results in an intrinsic loss of texture information, especially in the case of larger image scaling. The distance between the pixels from two consecutive sampling lines will obviously be apart when the sampling radius is closer to the boundary of the test image. Each projection line represents a feature that follows a single orientation with the corresponding angle. As a result, only the directional characteristics of the features can be preserved. For example, if there is a
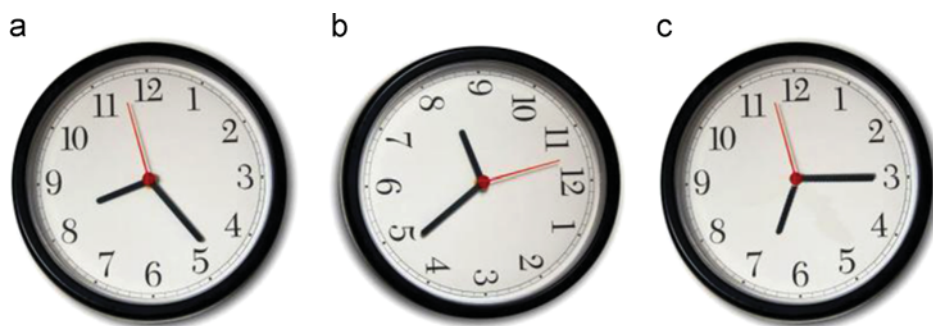

Fig. 1. An illustration of the circular symmetry problem: (a) original clock; (b) clock rotated; and (c) time changes.

strong edge perpendicular to the radial direction, it will be missed completely. If the projection profile is used to represent the actual texture characteristics of the template when attempting to solve the matching problem, then unpredictable errors are usually induced.

1.3. The goal of the paper

In this paper, we proposed a theoretically and computationally simple approach that is sufficiently robust to undergo RST variations and can be applied for realistic visual template matching application. A simple and well-defined feature map, the proposed SPLAM is illustrated to deal simultaneously with the rotation- and scaling-invariance transformation. The scale changes do not affect the appearance of the SPLAM. The rotation performed in the original image faithfully responds to the SPLAM when scrolled vertically. More specifically, when the original image suffers from a counter-clockwise rotation, the SPLAM rotates downwards. Similarly, if a clockwise rotation occurs, the SPLAM rotates upwards. The proposed SPM which provides structural and statistical information on the template in a more general and easier to comprehend format is presented here. Compared to the ring projection method the spiral-based projection provides a high level of sensitivity and scanning efficiency. As well, the inherent spatial information will be better preserved than by using the radial projection algorithm.

1.4. Contributions and organization

The contributions of our work are four-fold. (1) Based on the proposed image warping algorithm (i.e., SPLAM), the location finding and angle determination can be achieved quickly using the same model. (2) By taking advantage of the ring projection, the angle of the template rotation can be determined, and it also negates the possibly ambiguous rotation situation (i.e., circular

symmetry problem). (3) Compared with the radial projection, the analytic capability of spatial information is equally reported in each projection value. (4) A fast coarse-to-fine filtering method is proposed to determine the position and orientation of the reference template from the test image.

The remainder of this paper is organized as follows. Section 2 presents the proposed new descriptor: spiral projection and the image pixel aggregation method that is robust to rotation and scaling invariance. Experimental results are provided in Section 3 and finally we discuss our findings and draw our conclusion in Section 4.

2. The descriptor

A novel descriptor and fast algorithm for robust template matching was developed in this study. We proposed an efficient feature sampling scheme and aggregating model. Because one of the main characteristics of the spiral model is that it understands spatial variations, we used it to describe the local features of the template. The ultimate goal of this study was to develop an efficient template modeling method to solve/correct the template after it had undergone rotation, scaling, and translation variations. In addition, the proposed method has also been confirmed to be robust to the noise corrupted situations.

2.1. The proposed SPiraL Aggregation Map (SPLAM)

A constant-size feature map is constructed by collecting pixels from the original image regardless of the size of the image. The so-called SPiraL Aggregation Map (SPLAM) is created by the set of pixels on the spiral line with the corresponding angle from image space (u, v) to projection space (i, φ). Let $Splam(i, \varphi)$ denote the feature map sampled from the pixels along the spiral line at a rotation of φ degrees, and i denotes the index of the pixel sample.
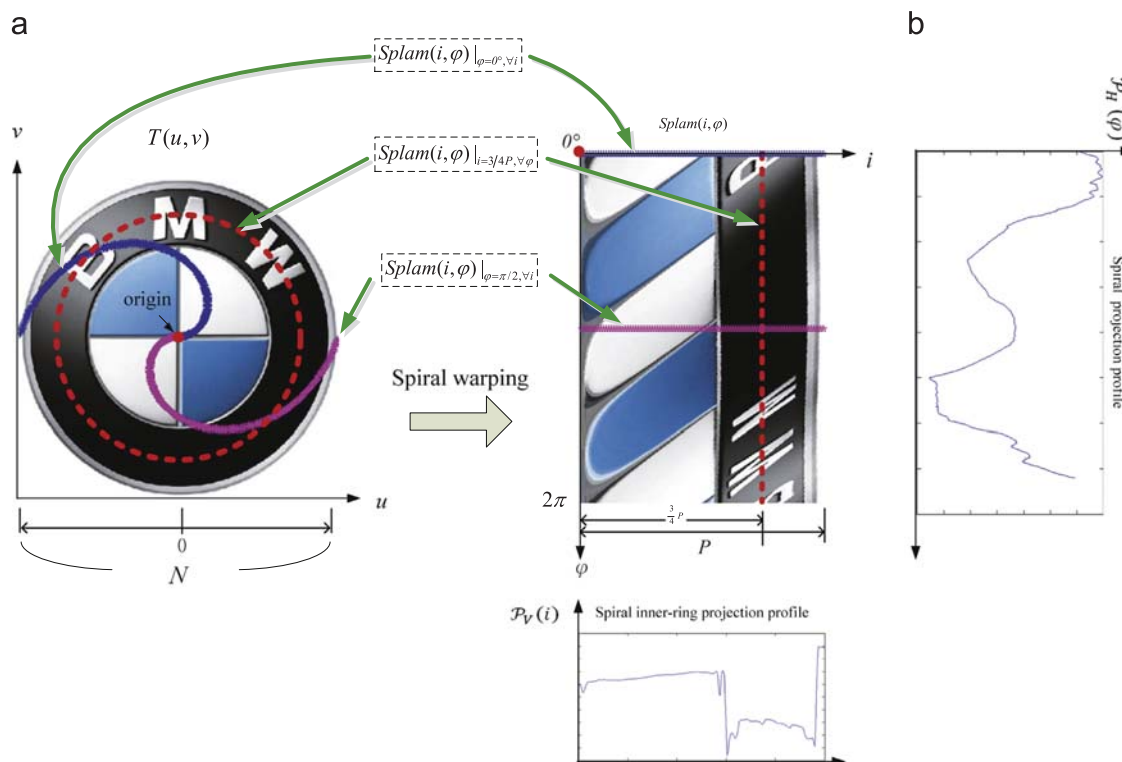

Fig. 2. Graphical illustration of the SPiraL Aggregation Map, $K=0.5$. (For interpretation of the references to color in this figure, the reader is referred to the web version of this article.)

Each group of sample pixels is vertically replaced into $Splam(i, \varphi)$ according to their angle φ. As mentioned above, $i = 1 \sim P$, where P is the number of sample pixels on each spiral line. Assuming that the spatial resolution of the spiral line is $\Delta\varphi$ degrees, we have $2\pi/\Delta\varphi$ sets of samples on each spiral line, rotating at φ degrees. Therefore, we can obtain a feature map with a fixed size of $2\pi/\Delta\varphi$ by P.

A conceptual illustration of the SPLAM construction is shown in Fig. 2. We draw two spiral lines in $\varphi = 0°$ and $\pi/2$ with blue and magenta star marks in Fig. 2(a). Each one is then sequentially arranged to the horizontal slice as shown in Fig. 2(b). To integrate all samples on each horizontal slice, we construct a spiral projection profile. The concentric circles with red dash marks denote the samples with the same serial number i on each rotated spiral line. In the feature map, this is displayed on the vertical slice with position i. To integrate all samples on each vertical slice, we construct a spiral inner-ring projection profile.

Based on the definition of the Archimedean spiral, the appearance of a spiral curve does not change with the size of the image. The SPLAM is scaling invariant, and we can extract the desired projection profiles from it. Let $\mathcal{P}_H$ denote the horizontal projection of the SPLAM, we have

$$\mathcal{P}_H(\varphi) = \left(\frac{1}{P}\right) \sum_{i=1}^{P} Splam(i, \varphi). \tag{1}$$

In addition, if $\mathcal{P}_V$ denotes the vertical projection of the SPLAM, which is composed by the spiral inner-ring pixels indexed by i, then we have

$$\mathcal{P}_V(i) = \left(\frac{\Delta\varphi}{2\pi}\right) \sum_{\varphi=0}^{2\pi} Splam(i, \varphi), \tag{2}$$

where $\Delta\varphi$ denotes the sampling offset in the rotation angle of spiral. In short, the SPLAM has two important properties: (1) It is scale-invariant: when the size of the test image changes, the horizontal and vertical projection profiles of SPLAM remain globally stationary. (2) It is rotation-distinguishable: if the image is rotated, it is reflected on the SPLAM by a vertical shift. The rotation angle can be determined by the vertical displacement of the feature map, and finding the maximal offset of the cross-correlation coefficient between the SPLAMs of the reference template and the test sub-image.

In next section, we consider how to find discrete finite samples along with the spiral expansion trajectory from the point of origin to the boundary of the image (or template).

2.2. Spiral projection model (SPM)

The geometric or Archimedean spiral, is named after Archimedes who explained that the spiral was the result of a point moving with uniform angular velocity and receding from the center (i.e., line velocity) at a constant rate. This paper is a model-based projection method, sampling pixels by using the spiral expansion model for both the template and the test sub-image. Based on the characteristics of spiral expansion, the sample evolution included both horizontal and vertical displacements simultaneously. This enabled it to preserve the fundamental structural information of the template.

According to the definition of Archimedean spirals [34], a continuous spiral trajectory can be described as

$$\rho_\varnothing = \alpha\varnothing \quad 0 \leq \varnothing < \infty, \tag{3}$$

where α denotes a constant describing the radial distance in a polar coordinate system, and $\rho_\varnothing$ is the distance from the point on the spiral line to the origin with the corresponding angle $\varnothing$. The trajectory can be formed as $\varnothing = 2\pi c + \omega$, where $c \in \mathbb{Z}$ indicates the number of laps, and ω is the angle of the x axis in the Cartesian-

plane, which can act as the angular velocity, periodically rotating with the origin point. To align the origin of the spiral trajectory with the Cartesian coordinate, we designed $\varnothing = 2\pi k$, where k denotes the number of laps, and $k \in \mathbb{R}$ in order to satisfy the requirement of the non-integer laps. Thus, the spiral line can be transformed onto the Cartesian-plane as

$$\begin{cases} u_\varnothing = \alpha\varnothing \cos \varnothing \\ v_\varnothing = \alpha\varnothing \sin \varnothing \end{cases} \quad 0 \leq \varnothing < \infty, \tag{4}$$

In order to deal with the scaling variation, we attempted to design a similar spiral line regardless of the size of the test sub-image. This provided a consistent sampling path from the point of origin (u_0, v_0) to the boundary of the image. The intrinsic texture features were preserved by the stationary sampled points on the reference template and test sub-image. Consequently it was important that the number of cycles after a certain evolution time remained unchanged. Fig. 3 shows a graphical illustration of the spiral sampling model. Let us consider two points $(\rho, \varnothing)$ and $(\rho', \varnothing + 2\pi)$ that are located in the same angle. If we apply for Eq. (3) then we have $\rho = \alpha\varnothing$, $\rho' = \alpha(\varnothing + 2\pi)$, and $d = |\rho - \rho'| = 2\pi\alpha$. Let d denote the smallest radial distance (i.e., radial interval) between these two points.

Suppose that the size of the image is $N \times N$, and K denotes the maximum number of laps from the point of origin to the boundary point, which is used to restrict the evolution of the spiral span. Let ρ_{max} denote the farthest point from the point of origin on the spiral line, that equals $N/2$, so that

$$\rho_{max} = dK = 2\pi\alpha K \tag{5}$$

Substituting $\alpha = \rho_{max}/2\pi K$ into Eq. (3) satisfies our requirement that the finite samples with the bound of expansion $\varnothing_{max} = 2\pi K$. Thus, we obtain a time-limited spiral line in the polar-plane,

$$\rho_\varnothing = \alpha\varnothing, \quad 0 \leq \varnothing < 2\pi K, \tag{6}$$

Based on the time-limited spiral function, we have a sample location (u_i, v_i) in the Cartesian plane,

$$\begin{cases} u_i = \alpha\varnothing_i \cos \varnothing_i \\ v_i = \alpha\varnothing_i \sin \varnothing_i \end{cases} \quad 0 \leq \varnothing_i < 2\pi K, \tag{7}$$

where $\varnothing_i$ denotes the corresponding angle arranged on $[0, \varnothing_{max}]$.

In the digital image, we need to find discrete samples along the spiral trajectory. A discrete approximation of the sample pixels along a spiral trajectory is given by the pre-defined K and the size of the image. Let $\mathbf{S}$ denote the collection of the spiral samples along the spiral trajectory from the reference template $T(u, v)$,
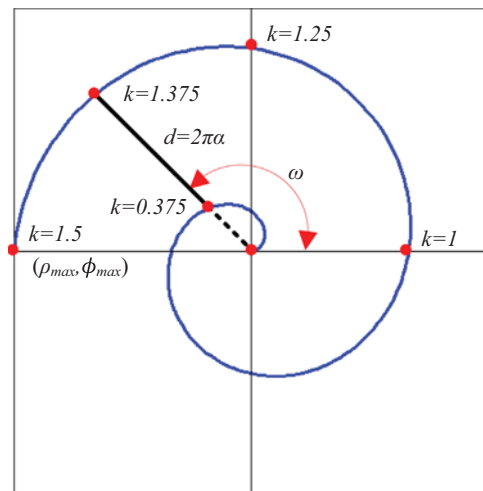

Fig. 3. Illustration of the spiral sampling algorithm.

expressed as

$$S \triangleq \{s_i\}|_{i=1\sim P} = \cup_{i=1}^{P} T(u_i, v_i) \tag{8}$$

where P denotes the amount of sampling points. The angular interval ω_j of the jth sample can be computed as follows:

$$\omega_j = \left(\frac{\theta_{max}}{P}\right)*j, \tag{9}$$

where j denotes the sample index.

Here, the value of the single spiral projection value on template T is defined as the mean of the intensities along the spiral trajectory centered at template T:

$$P_j = \left(\frac{1}{P}\right) \sum_{j=1}^{P} T(\alpha\omega_j \cos \omega_j, \alpha\omega_j \sin \omega_j). \tag{10}$$

Let φ define the angle of the counterclockwise rotation of the spiral trajectory around the center, and $\mathcal{P}^T(\varphi)$ denotes the projection profile of the template, which is constructed by uniform sampling of the whole template at angle φ,

$$\mathcal{P}^T(\varphi) = \left(\frac{1}{P}\right) \sum_{j=1}^{P} T[\alpha\omega_j \cos(\omega_j+\varphi), \quad \alpha\omega_j \sin(\omega_j+\varphi)]. \quad 0 \le \varphi < 2\pi \tag{11}$$

According to the characteristics of SPLAM, we can derive the projection profile using $\mathcal{P}^T(\varphi) = \mathcal{P}_H(\varphi)$, where $0 \le \varphi < 2\pi$. The major goal of the algorithm is to model the reference template and use it to estimate the rotation angle and scaling factor of test sub-image I_s with center location (x_s, y_s). Similarly, the projection profile for the test sub-image is formed as follows:

$$\mathcal{P}^{S(x_s, y_s)}(\varphi) = \left(\frac{1}{P}\right) \sum_{k=1}^{P} I_s\left[\left(x_s+d_x^k\right), \left(y_s+d_y^k\right)\right], \tag{12}$$

where (d_x^k, d_y^k) denotes the offset in the x- and y-directions along the spiral curve, respectively which is computed by

$$\begin{cases} d_x^k = \alpha\omega_k \cos(\omega_k+\varphi) \\ d_y^k = \alpha\omega_k \sin(\omega_k+\varphi). \end{cases} \quad 0 \le \varphi < 2\pi \tag{13}$$

The normalized correlation $\gamma(x_s, y_s)$ is defined in Eq. (14), which is used in the matching process to determine the similarity between the reference template and the test sub-image with center location (x_s, y_s).

$$\gamma(x_s, y_s) = \frac{\eta_s}{\|\mathcal{P}^T\| \cdot \|\mathcal{P}^S\|}, \tag{14}$$

where $\|.\|$ denotes the l-2 norm distance and η_s refers to the correlation between the reference template and the current test sub-image, which is defined as follows:

$$\eta_s = \sum_{\varphi=0}^{2\pi} \mathcal{P}^T(\varphi) \cdot \mathcal{P}^{S(x_s, y_s)}(\varphi). \tag{15}$$

The rotation angle can be determined by the offset τ which produces the maximal normalized cross-correlation value between the parametric template and test sub-image as follows:

$$\varphi^* = argmax_\tau\{\gamma(x_s, y_s), \tau\}, \quad \forall \tau \in \varphi. \tag{16}$$

2.3. Fast algorithm for template matching using SPM

For the sake of computational efficiency, a full search mechanism was not considered in this paper. Instead, we proposed the coarse-to-fine three-step filtering method to determine the position and orientation of the reference template T from the test image. Each sampling of sampled sub-image I_s from the test image is performed using the filtering algorithm.

2.3.1. Coarse filtering

We take advantage of the texture feature, and compute the variance of each spiral line with respect to the SPM indexed by angle φ as

$$\sigma^T(\varphi) = \left(\frac{1}{P}\right) \sum_{j=1}^{P} \left[T(\alpha\omega_j \cos \omega_j, \quad \alpha\omega_j \sin \omega_j) - \mathcal{P}_T(\varphi)\right]^2, \quad 0 \le \varphi < 2\pi, \tag{17}$$

which is formed as a vector with σ_{min} and σ_{max}. Let us consider that a boundary of reference template T is (d_x^k, d_y^k), and that N denotes the boundary of test sub-image I_s. Thus, the search range for the candidate center point is bound by $(d_x^k/2, d_y^k/2)$ and $(N-d_x^k/2, N-d_y^k/2)$. If a point located in the test sub-image has a variance value that is out of the range of $[\sigma_{min} \quad \sigma_{max}]$, it will be ignored. The variance of each spiral line can be calculated by

$$\sigma^S(\varphi) = \left(\frac{1}{P}\right) \sum_{k=1}^{P} \left\{I_s\left[\left(x_s+d_x^k\right), \left(y_s+d_y^k\right)\right] - \mathcal{P}_S(\varphi)\right\}^2, \quad 0 \le \varphi < 2\pi. \tag{18}$$

Considering the computational cost, we only applied the spiral line with angle 0° for test sub-image I_s, i.e., $\sigma^S(0)$. In short, when $\sigma^S(0) \in [\sigma_{min} \quad \sigma_{max}]$, the coordination of the corresponding center point is considered to be the candidate, and is stored in the candidate matrix $L[s_n]$ which represents the nth test point (x_n, y_n) in I_s. Let us assume that N_{cf} denotes the number of points after coarse filtering.

2.3.2. Interval filtering

Based on the results of the coarse filtering, interval filtering utilizes the interval information. Although it more complicated, it preserves more spatio-temporal information than the coarse filter. However, it also increases the computational cost. The coarse filter is only concerned with the projection profile along a single angle, while the interval filtering uses the interval relationships between more angles. The filtering procedure is extended to three other angles, 90°, 180°, and 270° for $L[s_n]$, where $n = 1 \sim N_{cf}$. The variances of these three spiral lines from the I_s, $\sigma^S(90)$, $\sigma^S(180)$, and $\sigma^S(270)$ are computed similar to the spiral line in coarse filtering. The variances are confirmed by interval σ^T at the same time. The point in candidate matrix L will be discarded if it does not satisfy the requirement of the interval filtering.

2.3.3. Spiral inner-ring filtering

The advantage of the SPLAM image is that scale changes do not affect the appearance of the SPLAM. Histogram equalization (HE) [16] is used to balance the local contrast variation between the template and the test sub-image. The rotation performed in the original image will reliably respond to the SPLAM with vertical scrolling. Therefore, we attempted to solve the problems of scaling and rotation simultaneously.

From the vertical aspect, the scaling and rotation variations will not affect the vertical projection of the SPLAM. For a given test sub-image, we first obtain $\mathcal{P}_V^{S(x_n, y_n)}(i)$ that forms the vector with 360 values (i.e., $\varphi = 0 - 2\pi$) on each candidate point n and the ith spiral inner-ring pixel by means of Eq. (2). When compared with the set of points on the reference template, i.e. $\mathcal{P}_V^T(i)$, if the average error of each point is less than the pre-defined constant β_1, then the corresponding feature score is added. The β_1 reflects the distinction between the mean of the spiral inner-ring projection on the test sub-image and the reference template. Let $F_v(n)$ denote the integral similarity score of the nth test point from $L[s_n]$, in other words:

$$F_V(n) = \sum_{i=0}^{P} u\left[\left|\mathcal{P}_V^{S(x_n, y_n)}(i) - \mathcal{P}_V^T(i)\right|, \beta_1\right], \tag{19}$$

where

$$u[A, B] = \begin{cases} 1 & \text{if } A < B \\ 0 & \text{if } A > B \end{cases}. \quad (20)$$

From the horizontal aspect, we can compute the horizontal projection $\mathcal{P}_H^{S(x_n, y_n)}(\varphi)$ of the test sub-image and $\mathcal{P}_H^T(\varphi)$ from the reference template using Eq. (1). Substituting $\mathcal{P}_H^{S(x_n, y_n)}(\varphi)$ and $\mathcal{P}_H^T(\varphi)$ into Eqs. (14)–(16), we find the best matched rotation angle φ^*. Based on the SPLAM characteristics these two horizontal projections satisfy the shift relationship. Hence, we can obtain the horizontal similarity score:

$$F_H(n) = \sum_{\varphi = 0}^{2\pi} u\left[\left|\mathcal{P}_H^{S(x_n, y_n)}(\varphi + \varphi^*) - \mathcal{P}_H^T(\varphi)\right|, \beta_2\right], \quad (21)$$

where β_2 denotes a pre-defined constant reflecting the distinction between the mean of the horizontal projection on the test sub-image and the reference template.

Finally, we sort the similarity score of both the vertical and the horizontal results. When the similarity scores F_v and F_H are both top-ranked, then the corresponding point will be preserved in L.

3. Experiments

In this section, five experiments were set up to evaluate the sensitivity and robustness of the proposed algorithm in performing template matching. First, the number of circles K of the spiral model was used to evaluate the sensitivity of the algorithm. In order to randomly rotate the test samples, the distinctive characteristics of the different SPMs with K must be identified. We also conducted experiments to test the sensitivity of the system for noise interference. Second, the robustness of the system for attacking the RST-variations was demonstrated. With different noises corrupting the images, the proposed SPM was still able to locate instances of accurate samples. Third, we compared the coarse-to-fine fast search method with the full search method for noise-free and noise corrupted situations. Fourth, the evaluation of the discriminating ability for circular symmetry template was examined. Finally, we compared our system to other methods.

3.1. Preliminary

For this study we collected the templates from a car logo, a university badge, and an official badge. There were a total of 20 templates used in the evaluation of the system, 5 from the car logo, 12 from the university badge and 3 from an official badge as shown in Fig. 4. The reference template was first selected and its center position defined. Before the SPM can be utilized, the vertex samples must be restored from the SPLAM feature space. This enables the system to generate robust feature descriptions for searching the sample instance of the test image and attack the RST deformation. We conducted a comprehensive representation of the template enabling us to determine the RST-invariant projection features.

The main purpose of template matching is to determine the accurate position and orientation of the template of the noise corrupted image. The center point of the sample instance can be estimated by the procedure shown in Section 2.3. As shown in Table 1, the pre-defined illumination change, contrast adjustment, and noise corruption are employed to support the robustness of the proposed system. All of the instance samples are set into a cluttered background image with random orientation and corrupted with different noise variations.

3.2. Sensitivity analysis of the spiral parameters

In the first experiment, we evaluated the sensitivity to distinguish the proposed SPM mechanism. In sampling the spiral model, the number of circles (i.e., K) in the spiral plays an important role in the degree of accuracy. Therefore, our aim was to test the sensitivity of the spiral parameter K using the rotation versions of the sample instances randomly embedded onto a cluttered background as shown in Fig. 5. From a statistics view point, we first computed the single spiral line over different K for each sample. The average value of 20 test images was estimated by means of entropy, homogeneity, and contrast computations. Fig. 6 shows the result of sensitivity test for the number of circle K, and ranged [0.1 5] with an interval of 0.1.

Based on this observation, when the circle of the spiral increases, the frequency of the entropy changes will decay, and the difference between the maximum and minimum value is reduced. This means that the projection profile of every single spiral line is depressed, inversely proportional to the circles of the spiral sampling. Apparently, the statistics of the homogeneity and contrast have the same tendency. Therefore, the smaller the K assignment, the higher the ability to distinguish. On the other hand, it is difficult to preserve the characteristics of the texture information when too large a circle of the spiral sampling is used.

We tested the template matching performance of the proposed SPM algorithm. To investigate the sensitivity of the proposed algorithm to the spiral parameter, the detection was performed by varying the K parameter to test the image datasets for intensity, contrast transformation, and a variety of noise, all on a cluttered background. To quantitatively measure the sensitivity of the proposed method, the true positive rate and a false alarm rate against the K values are shown in Figs. 7 and 8.

From Figs. 7 and 8, we can conclude that when the circle of the spiral increases, the accuracy of the template matching decays. Moreover, the error rate will increase at the same time. However, the circle of the spiral model (i.e., K) cannot shrink forever, and when K is selected to be less than 0.5, the true positive rate and the false alarm rate will show a similar performance. If the amount of corrupted noise is substantial, then the accuracy of the system performance is compromised, especially when K is less than 0.1. Therefore, the best K will range between 0.2 and 0.5. Based on our observations, the system performs best for the TPR measurement when K is 0.2. Nevertheless, the best performance for the FAR value is $K = 0.3$. In order to avoid missing the true instances, we applied $K = 0.3$ in the following experiments.

Noise corruption often reduces the efficiency of an image in the matching process. The intrinsic texture property of the image becomes distorted by the noise. Even when only the illumination is changed, the accuracy of the template matching is reduced, regardless of whatever well-defined model is being used. Compared with the full search scenario, and as shown in Figs. 7 and 8, the template matching performance of the fast coarse-to-fine filtering mechanism will be reduced by 20% of the TPR and increased by 25% of the FAR when K is less than 1.5. When K is greater than 1.5, the full search method will be increased by 30% of the TPR and reduced by 35% of the FAR. Nevertheless, the full search outperforms the fast search mechanism. The average computational cost of the full search is around 2.24 times that of the proposed coarse-to-fine search.

In addition, we found that the results of PN and GSF are relatively weak with the fast filtering method, and that they are not significant in the full search scenario. The major reason for this is that the true observation point is filtered out in the first-pass of coarse filtering. This is similar to the doping process, were a large number of noises are added to the spiral sampling step, resulting

Fig. 4. The template samples applied in the experiments: (a) the logos; (b) the badges; and (c) the official badges.

Table 1
The abbreviations of corrupted noises for the system evaluation.

Distortion type	Abbreviation	Demonstration
Illumination change	DI-10	Darken 10% of the intensity
	DI-20	Darken 20% of the intensity
	BI-10	Brighten 10% of the intensity
Contrast adjustment	DC-10	Depressed 10% of the contrast
	DC-15	Depressed 15% of the contrast
	EC-10	Enhanced 10% of the contrast
Noise corruption	GSF	*Gaussian smoothing filter* with 5×5 mask
	JPEG	*JPEG* compressed with 10% compression ratio
	SPN	Corrupted by *salt and pepper noise* with $p = 0.05$
	PN	Corrupted by *Poisson noise* with variance $= 0.5$

in the projection being in excess of the pre-defined range. On the other hand, the performances of the DI and EC produce good results with the fast filtering method, especially in the case of a large K. This implies that much of the uncorrelated information has been sampled in the spiral line. The less distinctive representations are summarized in the aforementioned entropy analysis. In addition, the proposed method is robust to the interference of the truncation error from the JPEG compression. The results achieved in the full search and the fast coarse-to-fine filtering mechanisms are similar.

Fig. 5. Test images of the sample instances for sensitivity analysis.

From the viewpoint of the FAR, the GSF produces worse results when a large K is chosen, because more noise has to be sampled. It should be noted that the noise corruption by GSF is very close to the original value. Therefore, many false candidates are detected in the full search method. Most of the erroneous points surround the true location, resulting in a significant increase in the false alarm rate. Although the fast coarse-to-fine filtering method enables the matching system to eliminate more errors, the number of false detections is higher than that in the full search. Overall, the higher the amount of the initial information the more the performance drops and the computational loading increases.

3.3. Robustness to the RST variations

To evaluate the robustness of the proposed method, a few vertex templates were created from the given reference template with different rotation angles and scaling factors with noise corruptions. In this experiment, two evaluations are demonstrated. For the first evaluation we set $K=0.3$ to test the robustness of the rotation-invariance. Each test image includes 5 instances with a fixed size as shown in Fig. 5. Then, we introduced noise into 20 test images to evaluation the system's accuracy of template matching. Three scaling factors {0.8, 1, 1.5} were used to evaluate the robustness of scale changes.

3.3.1. Rotation-invariance

In order to test the rotation-invariant property of the proposed fast search algorithm, we set $K=0.3$ for finding the location and orientation of the instances. Fig. 9 shows the result of each step of the filtering method. Fig. 9(b) shows the result of coarse filtering, where the blue pixels denote the valid center pixels of the candidate instances. The result of the interval filtering is shown in Fig. 9(c), indicating that a large amount of blue pixels was filtered out. When the 3rd step filter (i.e., spiral inner-ring filter) was used, five peaks of matching scores were obtained, as shown in Fig. 9(f). The corresponding center position and orientation are shown in Fig. 9(e).

In order to quantitatively measure the effectiveness of our proposed SPM method for dealing with the rotation, scaling, and translation transformations, we applied two commonly used metrics of precision and recall to describe the performance of the template matching algorithm. They are defined as follows:

$$\text{Precision} = \frac{TP}{TP+FP}, \quad \text{Recall} = \frac{TP}{TP+FN}, \quad (22)$$

where TP, FP, and FN denote true positive, false positive, and false negative respectively. However, when the recall rate is high, it is difficult to achieve a high precision rate, and conversely if the
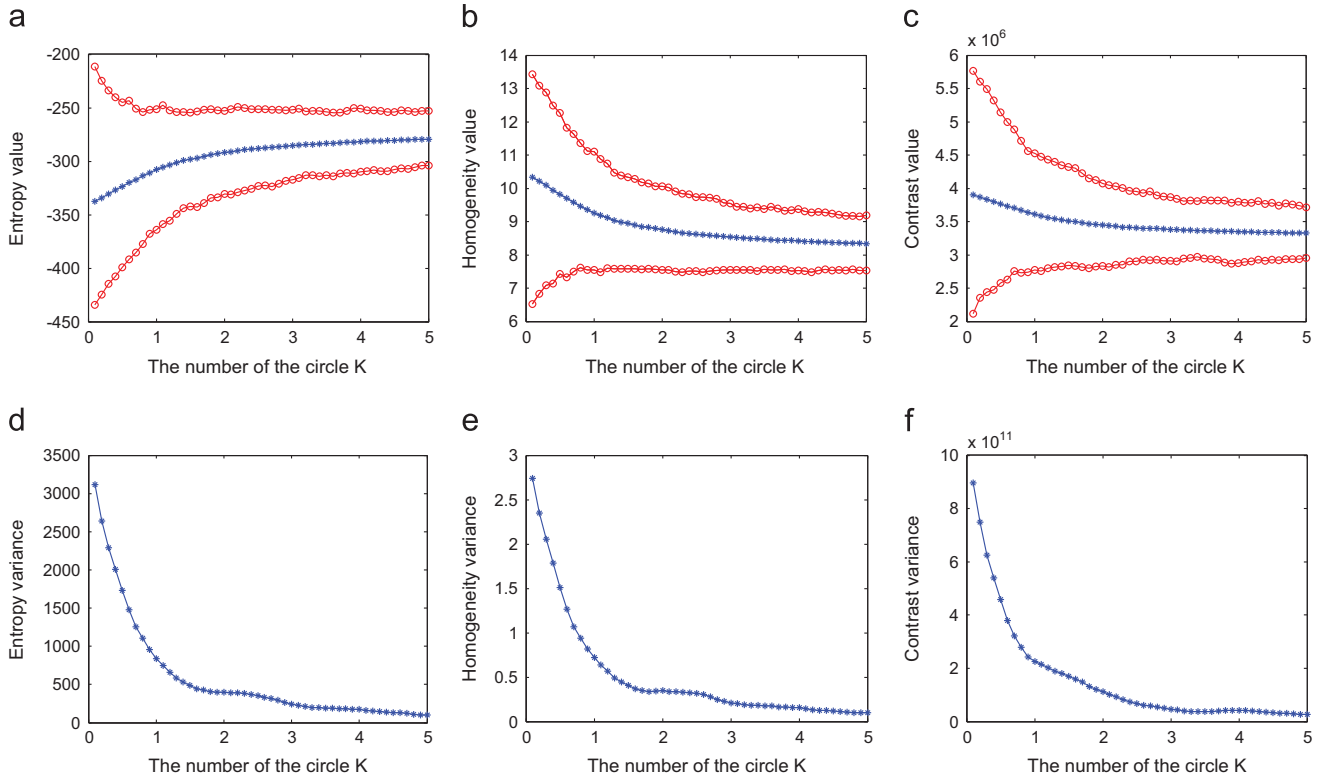
Fig. 6. Relationship between the number of spiral K and the average of the statistical value among each spiral sampling line: (a), (b) and (c) K vs. entropy, homogeneity, and contrast value, respectively. The red lines denote the maximum and minimum value, the blue line denotes the mean value. (d), (e) and (f) The results of the statistical variances of entropy, homogeneity, and contrast respectively. Each result is the average over the images shown in Fig. 5, and K ranged from 0.1 to 5 with an interval of 0.1. (For interpretation of the references to color in this figure legend, the reader is referred to the web version of this article.)

precision rate is high, it is impossible to have a high recall rate. Consequently, we used the F-measure to evaluate the overall performance as follows:

$$F - \text{measure} = 2 \times \left(\frac{\text{precision} \times \text{recall}}{\text{precision} + \text{recall}} \right). \tag{23}$$

Using the F-measure is the only way to obtain a high performance that simultaneously has a high precision and high recall rates. As shown in Table 2, the proposed method applied for testing the image datasets without the addition of noise achieved a performance of 91.79% in the F-measure. The overall precision rate is not very sensitive to illumination and contrast changes, which is less than 5% of the overall precision rate. It is still robust after the distortion of the high JPEG compression rate. An F-measure of approx. 85% can be reached when 90% of the data rate is truncated. The proposed descriptor and the fast search algorithm remain valid when corrupted with the salt and pepper noise. The worst result was obtained when Gaussian smoothing and Poisson noise were added. Even though, a high level of precision was maintained. The main problem is the low recall rate due to the fact that the test images have been depressed by the Gaussian and Poisson noises. Overall, the proposed matching algorithm achieved 84.97% precision rate and 78.75% recall rate when corrupted by the different noises. On an average, it achieved a performance of 83.45% when the three types of image distortions were applied.

3.3.2. Robust to scale changes

In this experiment, three scaling factors {0.8, 1, 1.5} were used to evaluate the robustness of scale changes. As shown in Fig. 10, each of the test images (sets) consisted of 4 logos with the corresponding SPLAM images. The vertex templates were generated based on the proposed image warping scheme as shown in Fig. 2. The same SPLAM images could be obtained for different scales of vertex templates. The resolution of the test image was 400×400. In all the different images, each logo was assigned a sign code. As shown in Fig. 11, the vertex templates with accurate scale factors, rotation angles, and the positions for test set 1 (with $K = 0.3$) were all detected correctly. More results are shown in Fig. 12.

In addition, we extended our experiment and tested the robustness for noise interference, such as listed in Table 1 (e.g. change in intensity, contrast adjustment, lossy JPEG compression, and some kernel noises). Fig. 12 shows the results of the scale-invariance experiment for the normal sample and template. The number and the orientation of the bounding box denote the sign code and rotation angle of the detected instance. Table 3 shows the performance of template matching with noise corruptions. Strictly speaking, the hit rate is only accumulated when the detected sample is recognized in the correct position, scale, and rotation angle simultaneously. A high level of accuracy can be achieved for a normal image, missing only one instance due to the corresponding template being undistinguishable. For illumination changes, an average hit rate of 86.11% is achieved and a hit rate of 88.33% is achieved for contrast changes. When it comes to noise corruption such as serious Gaussian smoothing and Poisson noise the performance is relatively weak. However, the template matching ability is relatively high for dealing with the artifacts of JPEG compression and salt and pepper noise. In short, our proposed system: (1) achieved a high level of precision for illumination and contrast changes, (2) was robust for blocking artifacts, which are a side-effect of JPEG compression, (3) achieved a 80% average hit rate for critical noise corruption.
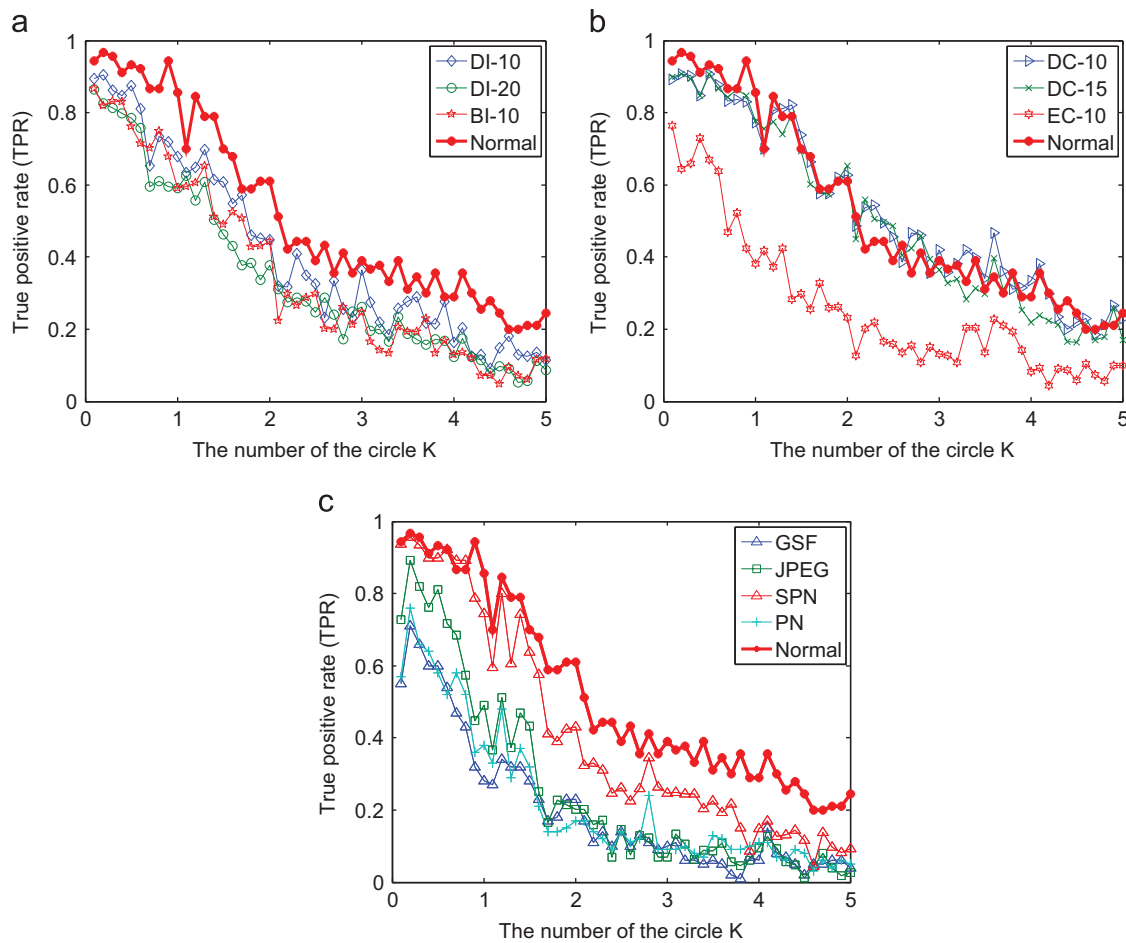
Fig. 7. TPR of different (a) illumination, (b) contrast, and (c) noise distortions for a varying number *K*.

3.4. Comparison with the full search method

In this paper, we proposed the coarse-to-fine three-step filtering method to determine the position and orientation among the instances in the test image. To test each pixel of the test image, the distribution of the matching score was obtained by using the pre-defined template model (i.e., SPLAM). This full search algorithm takes around 2.24 times more computation time than the fast search method. Based on our observation, only 12% of the pixels are left after the first two filtering steps (i.e., coarse and interval filters). However, the pre-defined range of variance of each spiral line with respect to the SPM might possibly be missed due to noise interference. In the coarse filtering step, especially the variance value is changed due to the uncorrelated pixel intensity being corrupted. To show the reliability of the proposed descriptor, we compared the performance of our proposed method with the full search mechanism for five types of noisy images with a relatively weak hit rate. Table 4 shows a high hit rate of template matching in the case of normal images (i.e., with noise corruption). This is the same weakness as when dealing with GSF distortion, because the smoothing operator induces many ambiguous pixels, in that it is unable to recover the accurate center position of the instances. On average, the fast search method had a hit rate that was approx. 1.6% less than that of the full search mechanism.

Figs. 13 and 14 respectively show the TPR and FAR comparisons between the fast and the full search mechanism for five types of noisy images with a relatively weak hit rate. For the number of circle *K* less than 1, the fast search method gained 0.1–0.2 in TPR and lost the same in FAR. However, a large *K* always performs worse due to the loss of intrinsic characteristics. In other words, the ratio of the computational time between a full and a fast search in EC-10, BI-10, GSF, JPEG, and PN is 4.47, 4.96, 2.16, 1.27, and 5.01 respectively. In Figs. 15 and 16, we compare the TPR and the average FAR (AFAR) for noise-free and noisy situations between the full and the fast search methods. Apparently, for the noise-free situation, the results of the TPR for both type of searches are very approximate (< 0.1) when $K < 2$. Also, the difference of AFAR between both searches is less than 0.1 when $K < 1$. When the noise is corrupted, the accuracy reduced by approx. 0.1 for the TPR measurement and increased 0.1 for the AFAR measurement for both search mechanisms.

3.5. Evaluation of the discriminating ability for circular symmetry template

To examine the robustness of the proposed method for circular symmetry template, we compared the discriminating ability of the SPM with other template matching methods. Comparing the rotation-invariance of the SPM with ring projection algorithm, we built 20 circular symmetry templates as shown in Fig. 17. These templates are similar to the original templates, but the center circular regions have been rotated. In Table 5, the results of comparison between the proposed SPM and ring projection model are shown. The recall rates were both high, but the precision of ring projection method was relatively low due to false positive detection. From the results of *F*-measure, it showed that our proposed SPM method is robust to the circular symmetry situation.
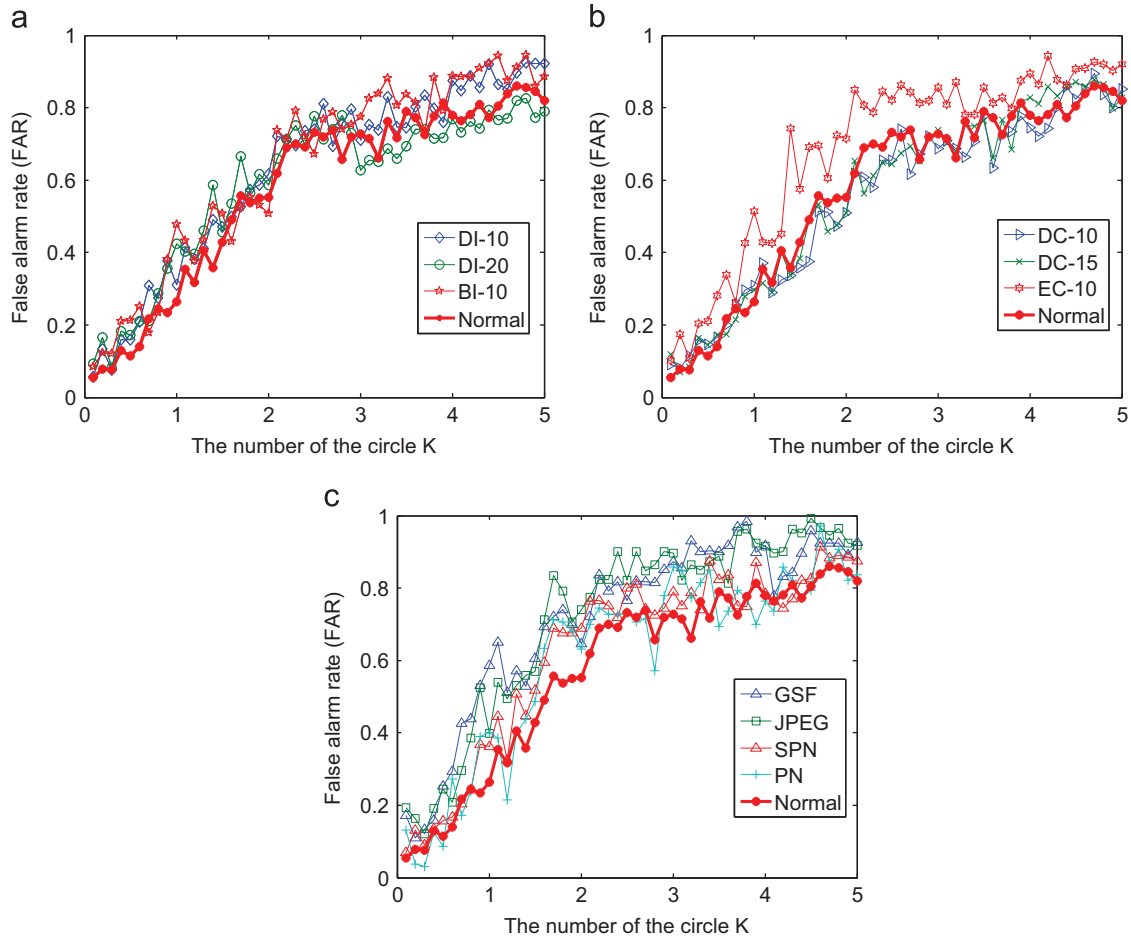
Fig. 8. FAR of different (a) illumination, (b) contrast, and (c) noise distortions for a varying number *K*.

3.6. Comparison with radial projection method

As aforementioned, a radial projection is a kind of extreme case of spiral projection. However, spiral projection method reserved more orientation information and texture properties about the image. In this section, we have conducted an experiment to demonstrate the accuracy using a particular number of radial and spiral sampling lines. More specifically, a part of spiral lines among 360° would be adopted to represent the template. Fig. 18 shows the comparison between spiral and radial projection methods using recall, precision, and *F*-measure indexes. This demonstrates that the recall rate of radial projection was significantly lower than that of spiral projection, especially when a small number of spiral lines was adopted. According to the result of *F*-measure evaluation, the spiral projection method outperforms the radial projection algorithm about 10% in accuracy. However, if more spiral lines being used, the more chaos will be induced. The number of sampling lines reflects the execution time as well. Consequently, it can be treated as a trade-off problem between computational cost and detection accuracy.

3.7. Comparison with state-of-the-art method

Previous studies have examined that the template matching algorithms can be divided into two groups: model-based and transformation-based approaches. Recently, the growth of research trends has focused on the mixed approach. For example,

Forapro (Fourier coefficients of radial projections) [30] is an efficient template matching approach. It uses the radial and circular features to detect the matching candidates. The normalized cross-correlation (NCC) is used to decide whether each of the matching candidates is a true or false matching result. Another possible filtering method is based on the generalized Hough transform [35]. However, it requires a set of stable sub-templates to against the partial occlusions. For the purpose of fairness, we compare our method only with the *Forapro-NCC* method.

We repeated the experiment of scale changes using the dataset in Ref. [30], including 24 memory game cards with 12 different figures. This dataset for testing the template matching algorithm is more challenging due to the high-corrupted background and greater scale factor ranges. In the beginning, 9 query templates were resized by scaling factors chosen randomly in the range [0.7 1.4], and pasted them in random non-overlapping locations to form eight test images. Table 6 depicts the number of observed errors using the *Forapro-NCC* and the proposed method, varying the number of candidate pixels n_c and the number of scales n_s. According to the results of Table 6, the proposed algorithm is capable of scale variations. To localize the template locations in the test image, the SPLAM with fast algorithm outperforms the *Forapro-NCC* method. For example, the number of matching candidates n_c represents the matching tolerance of the location offset. When a smaller value of n_c is assigned, it needs to search a pixel location more precisely. Based on our observations, with the same condition, i.e., $n_c = 10$, our method obtains less errors than *Forapro-NCC* method. Regardless of whether the n_c has been
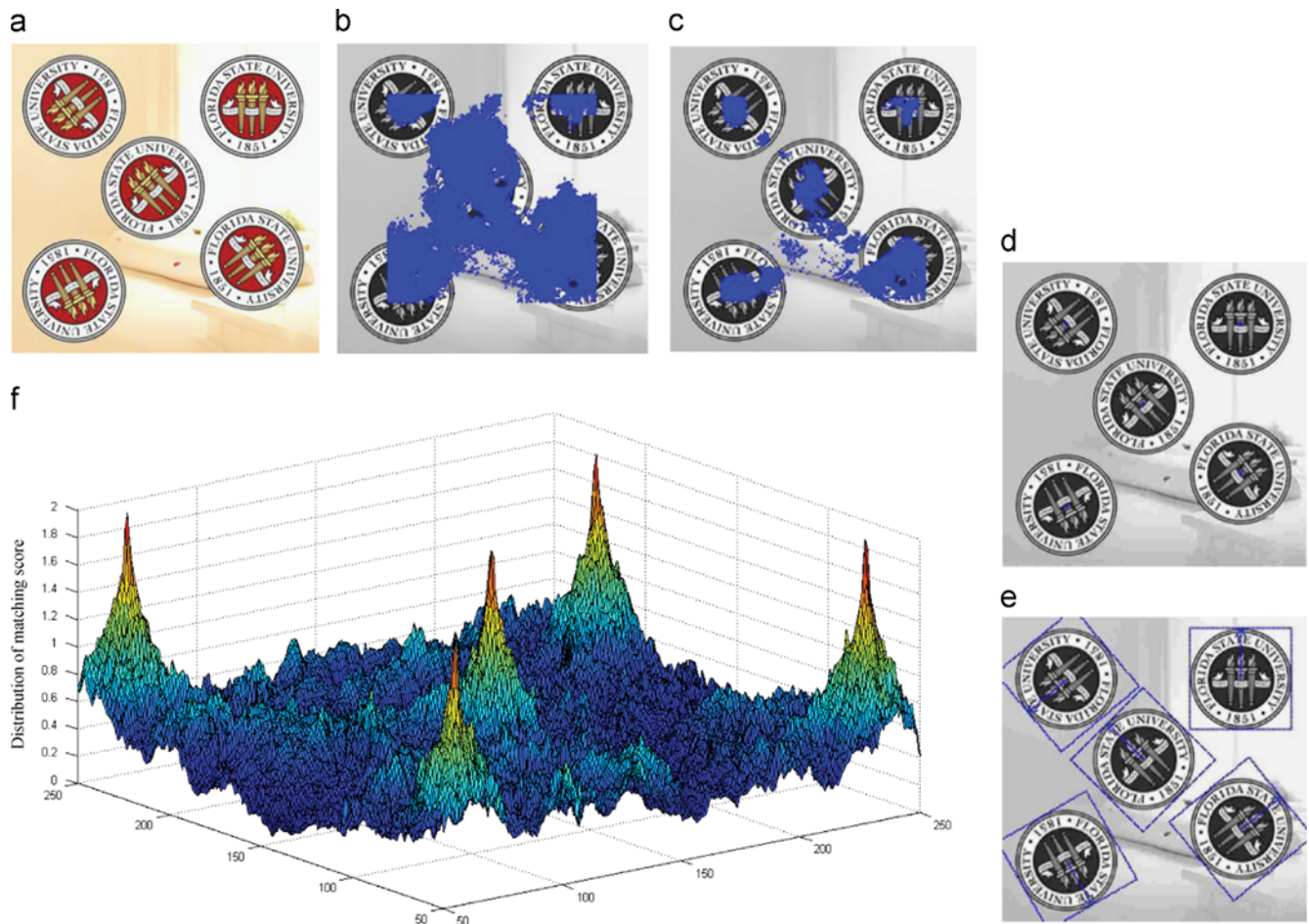
Fig. 9. Results of matching with the rotation variations: (a) original image; (b) result of coarse filtering; (c) result of interval filtering; (d) matching result by spiral inner-ring filtering; (e) detected logos with bounding box and orientation; and (f) matching scores (5 peaks denote the center location of the instances). (For interpretation of the references to color in this figure, the reader is referred to the web version of this article.)

Table 2
The matching performance with RST-variations for the proposed algorithm.

Noise	# Instances	True positive	False positive	False negative	Precision (%)	Recall (%)	F-measure (%)
Normal	**100**	**95**	**12**	**5**	**88.79**	**95.00**	**91.79**
DI-10	100	86	13	14	86.87	86.00	**86.43**
DI-20	100	81	14	19	85.26	81.00	**83.08**
BI-10	100	83	15	17	84.69	83.00	**83.84**
DC-10	100	90	17	10	84.11	90.00	**86.96**
DC-15	100	89	13	11	87.25	89.00	**88.12**
EC-10	100	66	13	34	83.54	66.00	**73.74**
JPEG	100	88	20	12	81.48	88.00	**84.61**
SPN	100	94	16	6	85.45	94.00	**89.52**
GSF	100	66	21	34	75.86	66.00	**70.59**
PN	100	67	2	33	97.10	67.00	**79.29**
Contrast adjusted	300	245	43	55	84.97	81.67	**82.94**
Illumination changed	300	250	42	50	85.61	83.33	**84.45**
Noise corrupted	400	315	59	85	84.97	78.75	**81.00**
Total/average	1100	905	156	195	**85.59**	**82.27**	**83.45**

assigned as 5 or 1 (i.e., exactly hit), the proposed method still be robust to scale changes.

3.8. Remarks on the experiments

In this paper, a new model-based descriptor taking advantage of both structural and statistical information was proposed. The algorithm of the descriptor was outlined as follows: First, a projection profile was constructed by sampling pixels along the time-limited spiral model. Second, the information implied in the projection profile was statistically integrated to form a feature vector. Third, a novel model-based image warping scheme was presented to build a feature map with fixed dimensions providing projection profiles for matching. The major advantage of the descriptor is that it enables scale- and rotation-invariance at the same time. It is also not susceptible to any change in illumination,

Fig. 10. Template images of the test sets and the SPLAM image with sign code (different resolutions).

Fig. 11. Result of template matching for 4 templates with RST variations ($K=0.3$).

contrast variation, or noise corruption. The results show that the proposed algorithm was successful in determining the real position of the template and acquired the precise angle of rotation of all the images.

4. Discussion and conclusion

The findings of this study could play an important role in developing an efficient template matching system to deal with unpredictable variations. The main contribution of this paper is the description of a simple and compact spiral-like feature descriptor which preserves structural and coherence information for image templates. By taking the advantage of the circular and radial projection, any variation in rotation and scaling of the template can be addressed simultaneously. The spiral projection model (SPM) was used to describe the texture feature of the template, and the SPiraL Aggregation Map (SPLAM) was proposed to determine the rotation angle of the template and effectively handle the scaling problem. It preserves more details of the reference template and enables us to deal more effectively with the rotation, scaling, and translation variations. The proposed feature representation method can be effectively treated as the index to retrieve the template location in a coarse-to-fine scenario for the test image. In our experiments we achieved many highly encouraging results for RST-invariant template matching applications.

The proposed descriptor is capable of expressing the template with high-order texture characteristics. The statistical discrimination can be accomplished by computing the statistics of the spiral line. The unobservable texels (texture elements) repeated in the template image can be measured by means of maximum probability, moments, contrast, homogeneity, entropy, energy and others. However, in order to reduce the complexity of the system, the second-order statistical

Fig. 12. More results of the scale- and rotation-invariance experiments.

Table 3
Performance in template matching for noise-corrupted images.

Noise	# Instances	True positive	False negative	Hit rate (%)
Normal	**60**	**59**	**1**	**98.33**
DI-10	60	53	7	88.33
DI-20	60	50	10	83.33
BI-10	60	52	8	86.67
DC-10	60	57	3	95.00
DC-15	60	56	4	93.33
EC-10	60	46	14	76.67
GSF	60	38	22	63.33
JPEG	60	55	5	91.67
SPN	60	59	1	98.33
PN	60	42	18	70.00
Contrast adjusted	180	159	21	88.33
Illumination changed	180	155	25	86.11
Noise corrupted	240	194	46	80.83
Total/average	660	567	93	**88.40**

Table 4
The performance of the full search mechanism for noise-corrupted images.

Noise	# Instances	True positive	False negative	Hit rate (%)
Normal	**60**	**60**	**0**	**100.00**
EC-10	60	53	7	88.33
BI-10	60	50	10	83.33
GSF	60	45	15	75.00
JPEG	60	58	2	96.67
PN	60	58	2	96.67
Total/average	360	324	36	**90.00**

characteristics of the texture information were observed only in this study.

On the other hand, this new descriptor does not use the color information as pixel density in the projection step. Color provides a powerful representation for pattern matching. If the color feature would be used, it could improve the overall performance of the system. However, using the color or not is a trade-off between computational burden and system accuracy in the matching process. Currently, we are developing a new model for matching image points of interest with a patch-based random
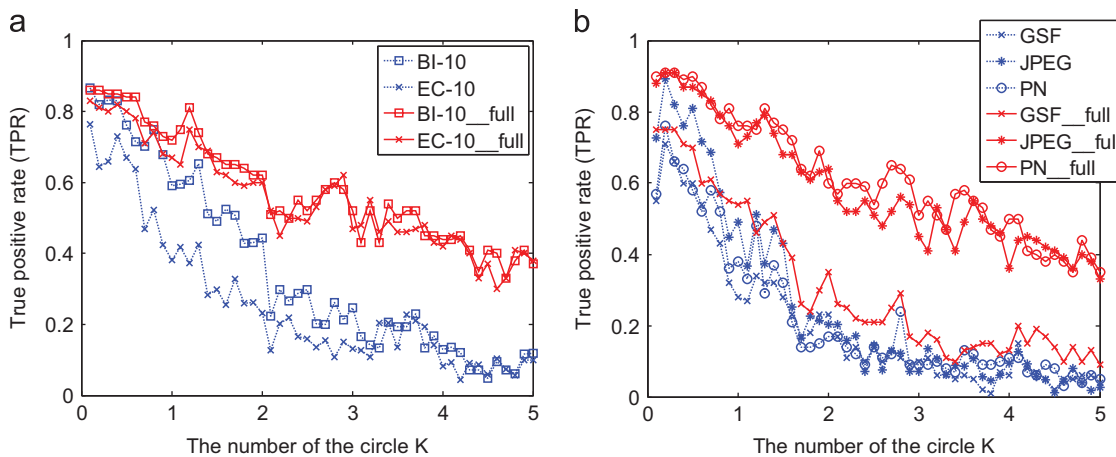
Fig. 13. Comparisons of TPR between the fast and the full search with different *K*: (a) illumination and contrast changes and (b) noise corrupts.
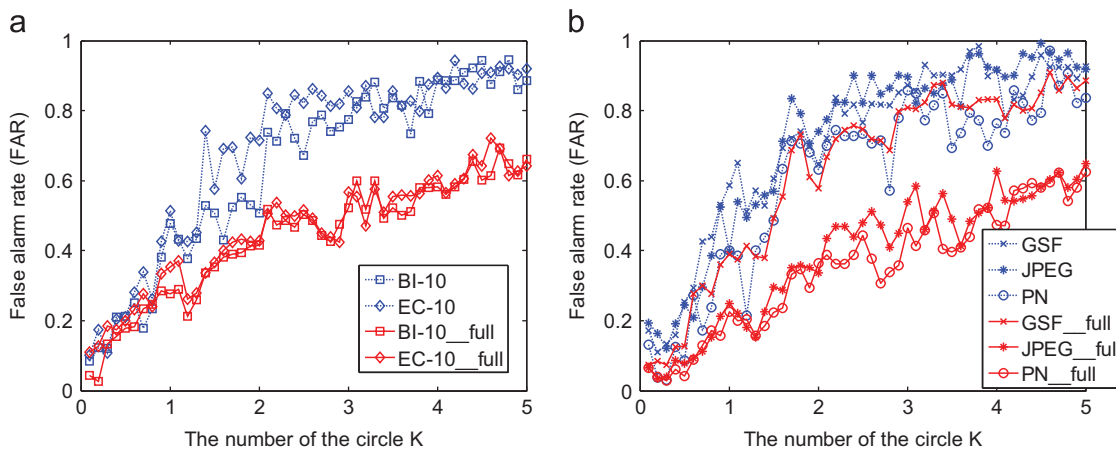

Fig. 14. Comparisons of FAR between the fast and the full search with different *K*: (a) illumination and contrast changes and (b) noise corrupts..
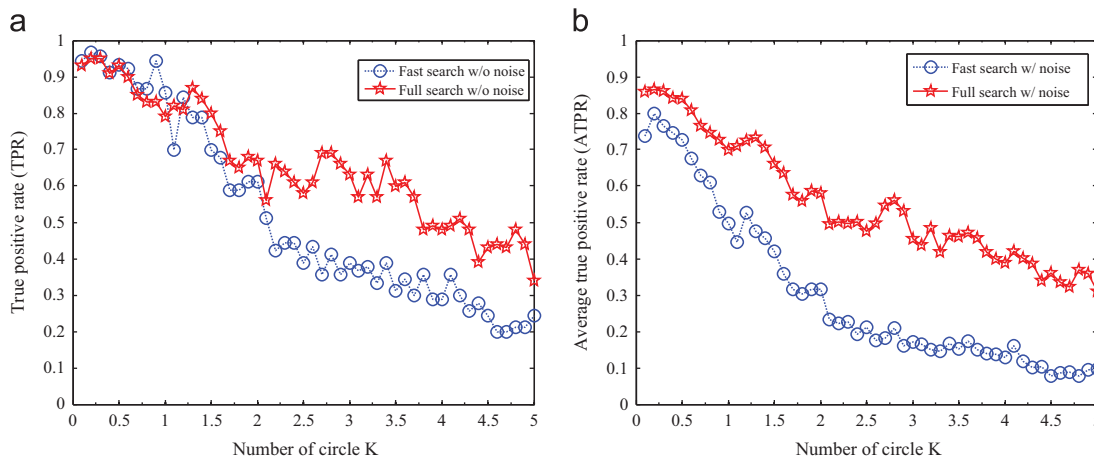

Fig. 15. (a) TPR comparisons between the fast and the full search without noise corruption and (b) the average TPR of the fast and full search with noise corruption.
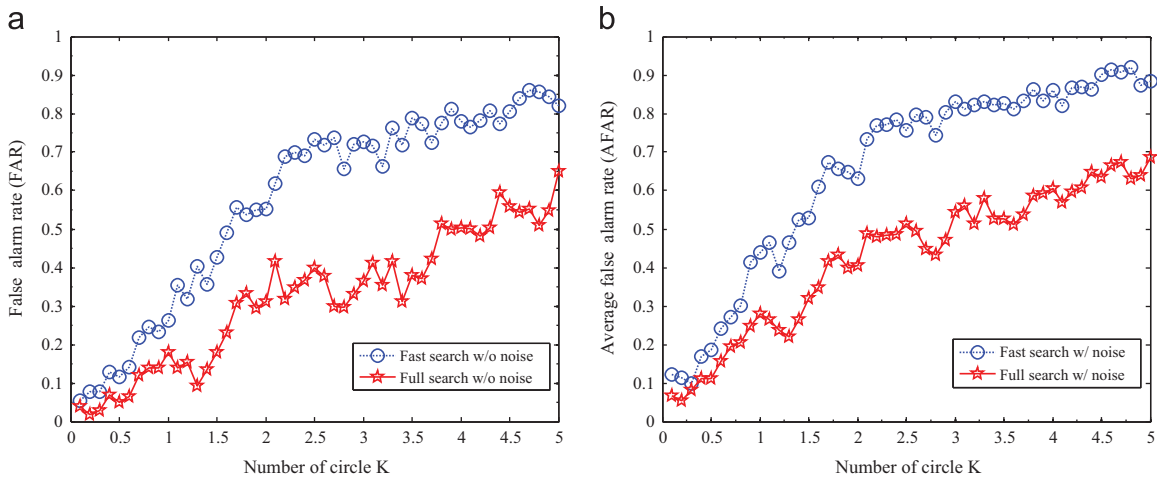
Fig. 16. (a) FAR comparisons between the fast and the full search without noise corruption and (b) the average FAR of the fast and full search with noise corruption.

Fig. 17. Examples of circular symmetry templates (the center part of template has been rotated).

Table 5
Performance comparison between spiral and ring projection models.

	# Instances	True positive	False positive	False negative	Precision (%)	Recall (%)	F-measure (%)
Spiral	20	20	3	0	86.95	100	93.02
Ring	20	20	20	0	50.00	100	66.67

color index for reducing the computational cost. We believe that the new model will provide resistance to partial occlusion and will not be sensitive to changes in the geometric transformations. Moreover, the proposed SPM can be easily modified for other types of spiral sampling. Our long-term goal is to investigate the possibility of 3D spiral projection for representing video data.
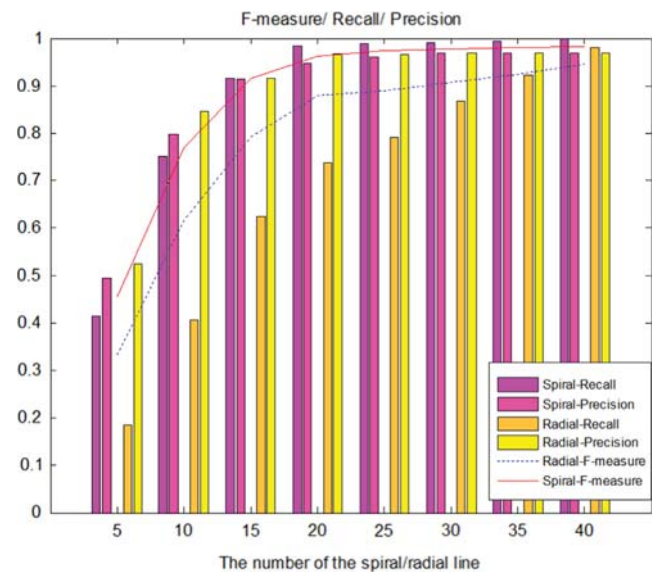
Conflict of interest

None declared.

Fig. 18. Performance comparison of the result of spiral projection and radial projection.

Table 6
Comparison between the proposed algorithm and *Forapro-NCC* on the robustness to scaling.

Errors (maximum=72)	SPLAM with fast algorithm					Forapro-NCC [30]		
	$n_c=1$	$n_c=5$	$n_c=10$	$n_c=20$	$n_c=45$	$n_c=10$	$n_c=20$	$n_c=45$
$n_s=4$	5	4	4	4	4	8	10	4
$n_s=5$	3	3	3	3	2	3	0	1
$n_s=6$	0	0	0	0	0	1	0	0
$n_s=8$	0	0	0	0	0	1	0	0

Acknowledgments

Appendix. Supplementary information

Supplementary data associated with this article can be found in the online version at http://dx.doi.org/10.1016/j.patcog.2014.11.004.

References

[1] H.Y. Kim, S.A. Araujo, Grayscale template-matching invariant to rotation, scale, translation, brightness and contrast, in: Proceedings of the Pacific-Rim Symposium on Image and Video Technology, Lecture Notes in Computer Science, Santiago, Chile, 2007, pp. 100–113.

[2] Y.Y. Tang, H.D. Cheng, C.Y. Suen, Transformation-ring-projection (TRP) algorithm and its VLSI implementation, Int. J. Pattern Recognit. Artif. Intell. 5 (1–2) (1991) 25–56.

[3] Y.Y. Tang, H. Ma, J. Liu, B. Li, D. Xi, Multiresolution analysis in extraction of reference lines from documents with graylevel background, IEEE Trans. Pattern Anal. Mach. Intell. 19 (1997) 921–926.

[4] M.-S. Choi, W.-Y. Kim, A novel two stage template matching method for rotation and illumination invariance, Pattern Recognit. 35 (2002) 119–129.

[5] S. Lin, C.-H. Chen, Template matching using the parametric template vector with translation, rotation and scale invariance, Pattern Recognit. 41 (2008) 2413–2421.

[6] R.L. Kashyap, A. Khotanzad, A model-based method for rotation invariant texture classification, IEEE Trans. Pattern Anal. Mach. Intell. 8 (4) (1986) 472–481.

[7] M. Tistarelli, G. Sandini, Dynamic aspects in active vision, CVGIP: Image Underst. 56 (1) (1992) 108–129.

[8] F. Ullah, S. Kanekoi, Using orientation codes for rotation-invariant template matching, Pattern Recognit. 37 (2) (2004) 201–209.

[9] S. Belongie, J. Malik, J. Puzicha, Shape matching and object recognition using shape contexts, IEEE Trans. Pattern Anal. Mach. Intell. 24 (24) (2002) 509–522.

[10] T. Ojala, M. Pietikaine, T. Maenpaa, Multiresolution gray-scale and rotation invariant texture classification with local binary patterns, IEEE Trans. Pattern Anal. Mach. Intell. 24 (7) (2002) 971–987.

[11] S.Z. Li, R.F. Chu, S.C. Liao, L. Zhang, Illumination invariant face recognition using near-infrared images, IEEE Trans. Pattern Anal. Mach. Intell. 29 (4) (2007) 627–639.

[12] A. Goshtasby, S.H. Gage, J.F. Bartholic, A two-stage cross correlation approach to template matching, IEEE Trans. Pattern Anal. Mach. Intell. 6 (3) (1984) 374–378.

[13] R. Bracewell, Fourier Analysis and Imaging, Kluwer, New York, 2003.

[14] B.S. Reddy, B.N. Chatterji, An FFT-based technique for translation, rotation, and scale-invariant image registration, IEEE Trans. Image Process. 5 (8) (1996) 1266–1271.

[15] D.-M. Tsai, C.-H. Chiang, Rotation-invariant pattern matching using wavelet decomposition, Pattern Recognit. Lett. 23 (2002) 191–201.

[16] R.C. Gonzalez, R.E. Woods, Digital Image Processing, Third edition, Addison-Wesley, 2008.

[17] A.G. Ramm, A.I. Katsevich, The Radon Transform and Local Tomography, CRC, Boca Raton, FL, 1996.

[18] K. Jafari-Khouzani, H. Soltanian-Zadeh, Radon transform orientation estimation for rotation invariant texture analysis, IEEE Trans. Pattern Anal. Mach. Intell. 27 (6) (2005) 1004–1008.

[19] F. Hjouj, D.W. Kammler, Identification of reflected, scaled translated, and rotated objects from their radon projections, IEEE Trans. Image Process. 17 (3) (2008) 301–310.

[20] M. Hazewinkel, Mellin Transform, Encyclopedia of Mathematics, Springer, 2001.

[21] R.N. Bracewell, The Fourier Transform and its Applications, 2nd ed., McGraw-Hill Book Co., Singapore, 1986.

[22] E.D. Castro, C. Morandi, Registration of translated and rotated images using finite Fourier transforms, IEEE Trans. Pattern Anal. Mach. Intell. 9 (3) (1987) 700–703.

[23] Q.S. Chen, M. Defrise, F. Deconinck, Symmetric phase-only matched filtering of Fourier–Mellin transforms for image registration and recognition, IEEE Trans. Pattern Anal. Mach. Intell. 16 (12) (1994) 1156–1168.

[24] D. Casasent, D. Psaltis, Position, rotation, and scale-invariant optical correlation, Appl. Opt. 15 (1976) 1793–1799.

[25] T.V. Hoang, S. Tabbone, Invariant pattern recognition using the RFM descriptor, Pattern Recognit. 45 (2012) 271–284.

[26] K. Jafari-Khouzani, H. Soltanian-Zadeh, Rotation-invariant multiresoultion texture analysis using Radon and wavelet transforms, IEEE Trans. Image Process. 14 (6) (2005) 783–795.

[27] G.Y. Chen, T.D. Bui, A. Krzyzak, Invariant pattern recognition using radon, dual-tree complex wavelet and Fourier transforms, Pattern Recognit. 42 (2009) 2013–2019.

[28] S. Zokai, G. Wolberg, Image registration using log-polar mappings for recovery of large-scale similarity and projective transformations, IEEE Trans. Image Process. 14 (10) (2005) 1422–1434.

[29] M. Amiri, H.R. Rabiee, A novel rotation/scale invariant template matching algorithm using weighted adaptive lifting scheme transform, Pattern Recognit. 43 (2010) 2485–2496.

[30] H.Y. Kim, Rotation-discriminating template matching based on Fourier coefficients of radial projections with robustness to scaling and partial occlusion, Pattern Recognit. 43 (2012) 859–872.

[31] Y.Y. Tang, B.F. Li, H. Ma, J. Liu, Ring-projection-wavelet-fractal signatures: a novel approach to feature extraction, IEEE Trans. Circuits Syst. – II: Analog Digit. Signal Process. 45 (8) (1998) 1130–1134.

[32] D.-M. Tsai, Y.-H. Tsai, Rotation-invariant pattern matching with color ring-projection, Pattern Recognit. 35 (2002) 131–141.

[33] P.C. Yuen, G.C. Feng, Y.Y. Tang, Printed Chinese character similarity measurement using ring projection and distance transform, Int. J. Pattern Recognit. Artif. Intell. 12 (1998) 209–221.

[34] [Online] Available: 〈http://mathworld.wolfram.com/ArchimedeanSpiral.html〉 (latest access time: 05.09.14).

[35] D.H. Ballard, Generalizing the Hough transform to detect arbitrary shapes, Pattern Recognit. 13 (2) (1981) 111–222.

Huang-Chia Shih received the B.Eng. degree with the highest honors in Electronic Engineering from the National Taipei University of Technology, Taipei, Taiwan in 2000 and the M.S. and Ph.D. degrees in Electrical Engineering (EE) from the National Tsing Hua University in 2002 and 2008, respectively.

He has been an Assistant Professor at the Department of EE, Yuan Ze University, Taoyuan, Taiwan, since 2010. His research interests are content-based multimedia processing, pattern recognition, and human–computer interaction (HCI). Dr. Shih served as Visiting Scholar in the Department of EE, University of Washington from September 2006 to April 2007, Visiting Professor in John von Neumann Faculty of Informatics, Obuda University in Hungary from July 2011 to September 2011. He received the Young Scholar Research Award from Yuan Ze University in December 2014, the Kwoh-Ting Li Young Researcher Award from ACM Taipei/Taiwan Chapter in April 2014, the Pan Wen Yuan Exploration Research Award from Pan Wen Foundation in May 2013, the best paper award of ISCE2013 from IEEE Consumer Electronics Society, the project of Outstanding Junior Research Investigators (2 years) from National Science Council in 2012, and the best doctoral dissertation from Image Processing and Pattern Recognition Society, Taiwan in August 2009.

Dr. Shih has published more than 40 technical papers in refereed journals and conference proceedings and served as a program committee member and reviewer for international journals and conferences.

Kuan-Chun Yu received the B.E. degree from the Department of Electrical Engineering, Yuan Ze University, Taoyuan, Taiwan, in 2013. His research interests are image morphological processing, image segmentation, and pattern recognition.